Feasibility Study of Particle-Assisted Laser Ablation of Brain Tumors in Orthotopic Canine Model

Jon A. Schwartz,[1] Anil M. Shetty,[2] Roger E. Price,[3] R. Jason Stafford,[2] James C. Wang,[1] Rajesh K. Uthamanthil,[2] Kevin Pham,[4] Roger J. McNichols,[4] Chris L. Coleman,[1] and J. Donald Payne[1]

[1]Nanospectra Biosciences, Inc.; [2]University of Texas M. D. Anderson Cancer Center; [3]Center for Comparative Medicine, Baylor College of Medicine; [4]Visualase, Inc., Houston, Texas

Abstract

We report on a pilot study showing a proof of concept for the passive delivery of nanoshells to an orthotopic tumor where they induce a local, confined therapeutic response distinct from that of normal brain resulting in the photothermal ablation of canine transmissible venereal tumor (cTVT) in a canine brain model. cTVT fragments grown in severe combined immunodeficient mice were successfully inoculated in the parietal lobe of immunosuppressed, mixed-breed hound dogs. A single dose of near-IR (NIR)–absorbing, 150-nm nanoshells was infused i.v. and allowed time to passively accumulate in the intracranial tumors, which served as a proxy for an orthotopic brain metastasis. The nanoshells accumulated within the intracranial cTVT, suggesting that its neovasculature represented an interruption of the normal blood-brain barrier. Tumors were thermally ablated by percutaneous, optical fiber–delivered, NIR radiation using a 3.5-W average, 3-minute laser dose at 808 nm that selectively elevated the temperature of tumor tissue to 65.8 ± 4.1°C. Identical laser doses applied to normal white and gray matter on the contralateral side of the brain yielded sublethal temperatures of 48.6 ± 1.1°C. The laser dose was designed to minimize thermal damage to normal brain tissue in the absence of nanoshells and compensate for variability in the accumulation of nanoshells in tumor. Postmortem histopathology of treated brain sections showed the effectiveness and selectivity of the nanoshell-assisted thermal ablation. [Cancer Res 2009;69(4):1659–67]

Introduction

The incidence of brain tumors in the United States, including primary and metastases of other cancers, is estimated to be around 200,000 per year (1). The incidence of brain tumors is reported to be increasing, although this may be due to enhanced detection techniques (2). Primary brain neoplasms account for ~10% of the total incidence, the majority of which (~75%) are classified as glioma or meningioma. The majority of brain tumors by far are metastases that most commonly arise from lung cancer (40–50%), breast cancer (15–25%), and melanoma (5–20%; ref. 3).

The management of brain tumors can be divided into symptomatic and/or therapeutic strategies. Symptomatic therapies primarily aim to decrease peritumoral edema and prevent recurrent seizures. Therapeutic modalities, on the other hand, aim to eradicate the brain cancer. The currently accepted treatment modalities for tumors of the brain include surgery, whole-brain radiotherapy, stereotactic radiosurgery (SRS), chemotherapy, or any combination of the above (3). Treatment regimens must take into account patient age, functional status, extent of systemic disease, tumor type and size, the number of tumors present, and prior therapies. For solitary masses under 3 cm in diameter, SRS has become the preferred treatment method. SRS uses multiple convergent beams to treat a discrete target area. Although it has eliminated surgical comorbidities by eliminating the need for an invasive intracranial procedure, radiotherapy still has significant complications, including early treatment-induced edema, seizures, and delayed radiation necrosis. There exists, then, the need for an effective treatment of solitary tumors that can avoid some or all of these problems.

We are investigating a particle-based, thermal ablative technique that offers significant promise in this area due to its potential to provide a high level of precision for tumor elimination while limiting or avoiding altogether radiotherapy-related complications. Particles are delivered i.v. and allowed to accumulate in the tumor by virtue of the enhanced permeability and retention effect, which characterizes the propensity for tumors to accumulate small particles and macromolecules from blood resulting from their poorly organized and fenestrated vasculature (4–6). Nanoshells (AuroShell particles, Nanospectra Biosciences, Inc.) used in this study are composed of a dielectric silica core encased in a thin gold shell with a total diameter of 144 to 150 nm. Nanoshells possess a plasmon resonance that imparts a large extinction coefficient over a relatively narrow band of the electromagnetic spectrum. The location of the plasmon resonance is dependent on the relative diameters of dielectric core and the gold shell (7, 8). By tuning the nanoshell resonance to the near-IR (NIR) region of the spectrum, the optical extinction of any tissue in which they accumulate may be greatly enhanced. Thus, illumination via a similarly tuned laser source may be used to preferentially heat nanoshell-bearing tissues.

Systemically administered nanoshells have previously shown a high selectivity for tumors and no extravasation into normal tissue, with particles cleared from the bloodstream by the reticuloendothelial system (9). When tumors accumulate nanoshells via enhanced permeability and retention, they may then be efficiently ablated with high selectivity over surrounding healthy tissues as seen in the effective elimination of solid tumors in several animal models (10–12). In addition, nanoshells have recently been used to induce mild hyperthermia in tumors and consequently enhance their susceptibility to radiotherapy in a human colorectal tumor model (13).

Requests for reprints: Jon A. Schwartz, Nanospectra Biosciences, Inc., 8285 El Rio Street, Suite 150, Houston, TX 77054. Phone: 713-842-2720, ext. 210; Fax: 713-440-9349; E-mail: jschwartz@nanospectra.com.

doi:10.1158/0008-5472.CAN-08-2535

Here, we present the results of a pilot study for the nanoshell-enhanced ablation in a canine transmissible venereal tumor (cTVT) brain tumor model. The two objectives of this study were to show the feasibility of ablation using a single dose of i.v. infused particles followed by a fixed laser dosimetry and to evaluate the need for real-time thermal monitoring to adjust laser dosimetry during the procedure.

Materials and Methods

Nanoshell fabrication. Nanoshell fabrication was based on the method of Oldenburg and colleagues (14). Briefly, gold colloids 1 to 3 nm in diameter were grown over an aminated, 120 ± 12 nm core of colloidal silica (Precision Colloids, LLC) using the method of Duff and Baiker (15). Gold colloid adsorbed to the amine groups on the surface of the silica core to form nucleating sites, which were then further reacted with $HAuCl_4$ in the presence of formaldehyde. This caused the surface colloid to grow and coalesce, ultimately forming a complete metal shell. Finished particles possessed a 12- to 15-nm-thick shell that resulted in an optical absorption peak between 780 and 800 nm. Thiolated polyethylene glycol (SH-PEG; Laysan Bio) was then assembled onto nanoshell surfaces by combining 1 mmol/L SH-PEG and nanoshells in a ratio of 1.5 μL/mL in deionized H_2O for 12 h followed by diafiltration to remove the excess SH-PEG. Particles were then suspended in 10% trehalose solution to create an iso-osmotic solution for injection and concentrated by transverse flow filtration to an extinction of 100 ± 5 absorbance (at 800 nm) to reduce the infused fluid volume. Nanoshells were fabricated under clean conditions in a class 100 clean room and passed through a 0.45-μm filter.

We based the nanoshell dosing level on extensive prior research in rodents.[5] We arrived at an optimal nanoshell dose determined from NAA-derived nanoshell accumulation in allografted tumors. The optimal nanoshell dose, corresponding to 1.25e9 nanoshells/gram of body weight, was scaled up for this study by the estimated blood volume for mongrel dogs versus mice (5.2 versus 4.5 mL/kg; ref. 16).

cTVT propagation. All animals were handled in accordance with Association for Assessment and Accreditation of Laboratory Animal Care and Office of Laboratory Animal Welfare guidelines under the direction of the Institutional Animal Care and Use Committees at Nanospectra Biosciences and The University of Texas M. D. Anderson Cancer Center. cTVT is a naturally occurring transplantable round cell tumor in dogs (17, 18). Because cTVT spontaneously regresses in healthy dogs, its growth and propagation requires an immunosuppressed host. Fresh cTVT fragments from the Department of Veterinary Medicine and Surgery at the M. D. Anderson Cancer Center were finely minced and inoculated via 20-gauge needle into the flank and nape of severe combined immunodeficient (SCID) mice, which yielded the additional benefit of producing tumors containing much less intermingled connective tissue than when grown in canines. Tumors required 4 to 6 wk to mature into a ~1-cm-diameter mass, whereupon they were harvested for either canine inoculation or propagation into a new mouse.

cTVT canine model. Nine mixed-breed hound dogs, three males (~29 kg each) and six females (~22–25 kg each), were obtained by the Department of Veterinary Medicine and Surgery at the M. D. Anderson Cancer Center from the University of Texas Health Science Center/Houston. All dogs were acclimated for at least 7 d and then begun on a course of cyclosporine (Sandimmune, Novartis Pharma SAS) at a dose rate of 10 mg/kg twice daily for 10 to 12 d. Before surgery, the dogs were placed on a course of antibiotics (cefazolin, 20 mg/kg) and analgesia (Buprenex, buprenorphine hydrochloride, 0.02 mg/kg). At the time of surgery, the dogs were induced with a ketamine/midazolam (Versed) solution (ketamine, 10 mg/kg; midazolam, 0.5 mg/kg; and glycopyrrolate, 0.01 mg/kg), incubated, and maintained with a 2% isoflurane/oxygen mixture.

After each dog was sterile prepped and draped, an incision was made along the coronal ridge down to the skull. The skin and underlying muscle was freed and retracted, whereupon two twist drill holes were drilled and tapped bilaterally in the cranium above the parietal lobes of the brain. Magnetic resonance imaging (MRI)–compatible threaded Temporary Bone Anchors (Visualase, Inc.) were screwed into each twist drill hole to provide a reproducible means of inserting a surgical catheter and to stabilize and secure the biopsy needle during inoculation. A 14-gauge cannula was inserted in the Bone Anchor opening. The 14-gauge cannula was cut to length so that it extended 15 mm beneath the dorsal surface of the cerebral hemisphere. An 18-gauge biopsy needle was inserted through a cannula in the Bone Anchor (Fig. 1*A*) to a point 17 mm below the dorsal surface of the cerebrum and secured in position. Tumor inoculation was performed in one parietal lobe by inserting the biopsy needle, slowly expelling approximately 6 to 7 μL of cTVT fragments, and rotating the needle several times to detach any adherent tumor from the end of the needle. A sham inoculation was made into the contralateral parietal lobe. After completion of the inoculation procedures, the Tuohy-Borst adapter was removed and the Bone Anchor orifice was filled with bone wax after being flushed with saline. The incision in the masseter muscle and skin was then closed and sutured. An additional inoculation of tumor fragments was injected s.c. on the flank of each dog to serve as an external palpable index for tumor growth.

Postsurgical care included antibiotics (Simplicef, cefpodoxime proxetil, 10 mg/kg), analgesia (Buprenex, 0.02 mg/kg), a nonsteroidal anti-inflammatory (meloxicam, 0.2 mg/kg postoperatively and 0.1 mg/kg for 1–2 d postoperatively), and periodic observation for neurologic symptoms. Cyclosporine was continued at 10 mg/kg once daily from the day of inoculation until sacrifice. Tumors were allowed to grow until their major axis approached 1 cm in length, typically at 6 to 8 wk when their presence was confirmed using magnetic resonance-dynamic contrast enhancement (MR-DCE). When an appropriately sized tumor was confirmed, the dog was scheduled for nanoshell infusion and laser treatment.

Laser and water-cooled, percutaneous laser applicator. NIR radiation was provided by a high-power diode laser (15*plus*, Diomed, Inc.) delivered percutaneously via a water-cooled diffusing optical fiber applicator, the Visualase Cooled Laser Applicator System (VCLAS), shown in Fig. 1*B*. Calibration of the laser output power was accomplished using a calibrated integrating sphere optometer (P9710-2, Gigahertz-Optik, GmbH). The laser was a 15-W gallium arsenide diode unit emitting at 810 ± 20 nm in continuous or pulsed modes. This wavelength is within the NIR "therapeutic window" (~700–1,300 nm) that minimizes endogenous absorption by oxyhemoglobin and deoxyhemoglobin, maximizing optical penetration through vascularized tissue (19, 20), and is simultaneously near the absorption peak of the nanoshells. Within the dual lumen of the VCLAS was an optical fiber terminated with a 1-cm-long isotropic diffusing tip. The diffuser provides highly uniform emission longitudinally and radially. The VCLAS permitted minimally invasive access to orthotopic tumors and the water-cooled applicator is effective at increasing the treatment depth by cooling tissue proximate to the fiber, which would normally be the first to denature, limiting subsequent light penetration.

MRI temperature monitoring and Visualase thermal mapping system. MRI was used to monitor spatially resolved temperatures *in vivo* based on the temperature-dependent proton resonance frequency shift. Complex phase-difference images from a temperature-sensitive interleaved gradient-echo, echo-planar imaging sequence were processed to display temperature by the Visualase system (21). The system interfaces with the MRI via Ethernet and uses information derived from temperature-sensitive MRI images to provide near real-time temperature mapping of the MR images (22). The system allows an operator to closely follow the thermal therapy by monitoring real-time MR images simultaneously overlaid with a false-color map of temperature and modeled Arrhenius thermal ablation zones (17).

Photothermal ablation. The laser dosimetry used for all of the cases presented here was developed in previous studies in mice and rats. We found that 3.5 W of 808-nm light, delivered from the 1-cm isotropic diffusing fiber with a duty factor of 75% for 3 to 4 min, was at or just below the threshold for producing thermal ablation in vascularized tissue. We

[5] D.P. O'Neal and K. Gill-Sharp, unpublished data.

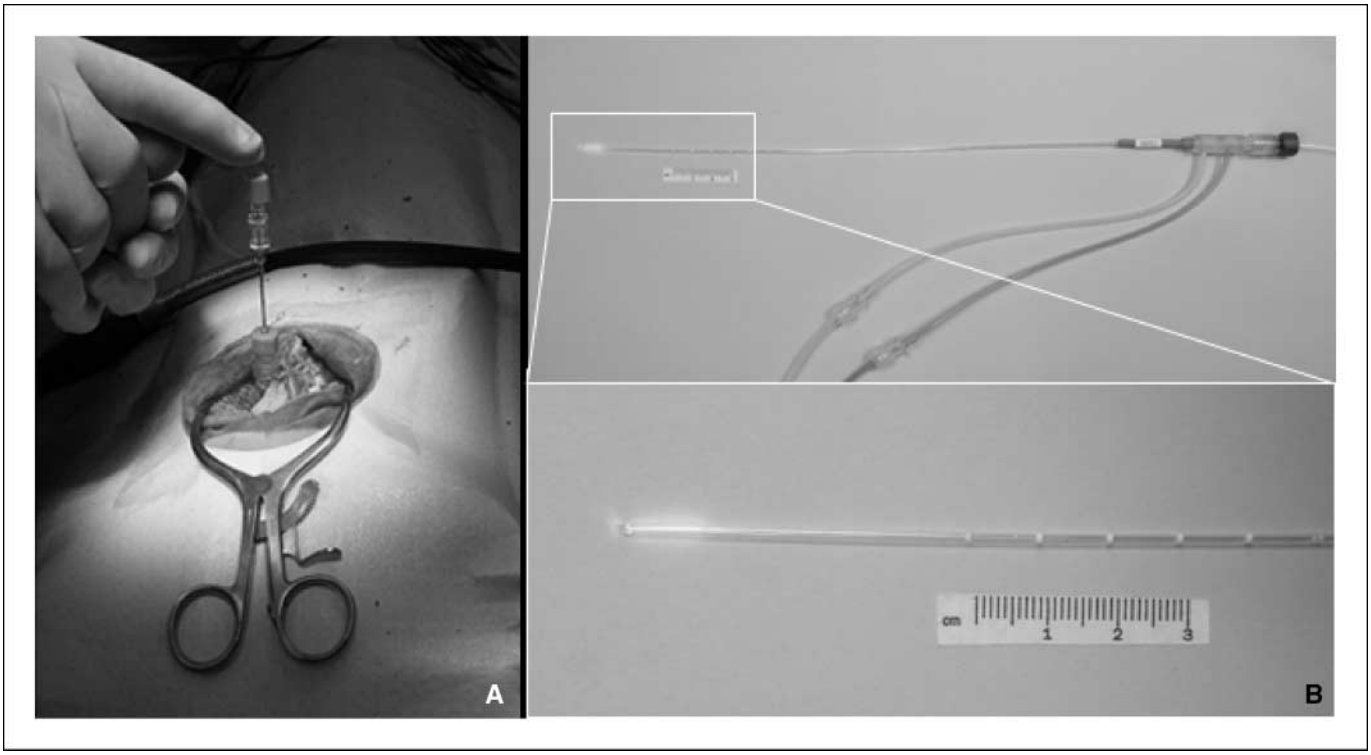

Figure 1. *A,* inoculation of cTVT cells into the parietal lobe of a dog brain. An 18-gauge biopsy needle filled with cTVT fragments is shown inserted through and secured by a Bone Anchor. *B,* a 16-gauge × 11-inch VCLAS; a 400-μm core optical fiber terminated with a 1-cm-long isotropic diffuser is shown (*inset*) illuminated at the distal end of the VCLAS.

attribute the difference in thermal ablation volumes between the nanoshell and vehicle control brains detailed here to the presence or absence of nanoshell accumulation.

The s.c. cTVT tumors were monitored in the dogs as an index for brain tumor growth. When these tumors became palpable, the dogs were anesthetized and taken for MR evaluation of their brain inoculations. Brain tumors were detected by MR-DCE using gadopentetate dimeglumine (Magnevist, Bayer Pharmaceuticals) as a contrast agent. The contrast agent changes the homogeneity of the magnetic field in the surrounding tissue and results in a marked decrease in $T2^*$ relaxation time. As the bolus passes through a region of interest, the signal from that region is attenuated as a result of spin dephasing. The signal returns to normal after the bolus has passed (23).

Dogs receiving nanoshells were i.v. infused with 5.2 mL/kg of 100 absorbance nanoshells at a rate of 2 mL/min for 5 min, subsequently increased to 5 mL/min for the duration. Dogs used as controls received the same dose and rate of the vehicle (10% trehalose). Twenty-four hours after nanoshell infusion, dogs were anesthetized as before, the cranial incision was reopened, the Tuohy-Borst adapters were rethreaded into the Bone Anchors, and the dogs were taken to the MR suite. There, they were imaged by MR-DCE to confirm the presence and location of the previously observed tumor. Using sterile technique, the VCLAS cooled catheter was inserted through and secured by the Bone Anchor, positioning the optical fiber within the brain at the level of the tumor. A series of temperature-sensitive echo-planar imaging sequence MR images were collected at 6-s intervals, whereas the laser was activated at 3-W output for 30 s. Localized heating was measured by this imaging sequence using the real-time thermal mapping system, which permitted verification of the location of the optical fiber diffusing tip relative to the desired target. The catheter was adjusted as necessary to bring it in good proximity to the tumor. We carried out the photothermal treatment in the same manner, recording magnetic resonance thermal imaging (MRTI) data, which were displayed in real time as the laser was energized at 3.5 W_{avg} for 3 min. After laser treatment of the tumor, the laser catheter was removed and reinserted through the contralateral Bone Anchor into normal brain and an identical laser treatment was performed. After photothermal treatment, another series of MR-DCE images were recorded to assess acute changes in blood perfusion in the treated areas of the brain. Forty-eight hours after laser treatment, dogs were anesthetized and imaged to assess short-term resolution of the thermal injury. The dogs were then sacrificed under anesthesia for necropsy examination and tissue harvest. Harvested tumor and brain tissue samples were obtained for histopathology and neutron activation analysis for gold content as a measure of particle uptake. The intact brain and tumor samples were fixed by immersion in a 10% buffered formalin solution for a minimum of 96 h before slicing and documentation of the extent of the thermal damage.

Neutron activation analysis. Tissue samples containing gold-bearing nanoshells were assayed *ex vivo* using neutron activation (or elemental) analysis (EA). EA for these studies, conducted by the Nuclear Engineering Teaching Laboratory at the University of Texas at Austin, uses neutron bombardment to excite stable gold $_{79}Au^{197}$ to the radioactive $_{79}Au^{198}$. This radioactive isotope decays with a half-life of 2.7 d, emitting characteristic 412 keV γ-rays that were used to quantify gold content. We used the EA-measured gold and tissue mass to derive gold concentrations in tested tissues. Calculating the expected mass of gold per nanoshell yields an estimate of the number of particles present.

Results

The key features of the nanoshell infusion and laser treatment are summarized in Table 1. Of the nine dogs inoculated with cTVT, only five grew intracranial tumors. Of those with tumors, four received nanoshells and photothermal ablation (dogs 1–4 in Table 1) and one received laser illumination but no nanoshells as a control (dog 5 in Table 1). Of the four dogs that did not grow tumors, three were withdrawn from the study and one served as a healthy control (dog 6 in Table 1) for photothermal ablation in the

Table 1. Heating plateau temperatures, change in temperature, and EA-derived gold concentrations for key experiments

Animal no.	Tissue	Lesion maximum temperature plateau (°C)	ΔT at lesion core (°C)	Tissue gold concentration (μg/g)
Tumors with nanoshells				
1	Intracranial tumor	64.9	27.9	49.3
	White matter	49.6	12.6	0.24
2	Intracranial tumor	64.8	27.7	Not available
	White matter	57.1	20.4	Not available
3	Intracranial tumor	61.9	27.2	2.8
	White matter	49.3	15	0.043
4	Intracranial tumor	71.5	34.9	15.5
	White matter	47.5	10.6	Not available
Tumor, no nanoshells				
5	Intracranial tumor	53.1	17.6	
	White matter	49.3	14.4	Not available
No tumor, no nanoshells				
6	—	—	—	
	White matter	47.4	11.7	Not available

brain. There were no significant neurologic issues after any intracranial procedure with the exception of one dog, which had a single seizure during recovery from anesthesia immediately following laser treatment. This dog recovered immediately and stayed free of seizures or other neurologic problems for the remainder of the study. No signs of neurologic damage were observed in other dogs after laser treatment and before sacrifice.

Laser illumination was applied from a single fiber insertion, although in two cases (dogs 3 and 6 in Table 1) the fiber was retracted within the cooled catheter to treat multiple sites along the fiber track. In two cases (dogs 2 and 3 in Table 1), we observed hemorrhage during the laser illumination of the nontumored hemisphere. In both cases, the hemorrhage occurred at the base of a sulcus and seemed to result from the insertion of the optical fiber catheter rather than as a result of laser illumination. The maximum temperature achieved in any MRTI pixel is indicated in Table 1.

The extent of the thermal coagulonecrosis was evaluated using H&E-stained sections of formalin-fixed brain tissue approximately 48 hours after the thermal insult. Unlike other tissues in the body, tissues of the central nervous system characteristically undergo relatively rapid liquefactive necrosis following a lethal insult (24). Immediately following lethal thermal irradiation, the brain and other tissues typically undergo coagulative necrosis characterized by preservation of the previous tissue structure and architecture. The 48-hour time period was found in previous studies to allow maximum progression of the necrotic process before liquefaction and loss of histologic evidence of prior normal tissue structures and tumor.

We will discuss two relevant cases in detail: dog 4, which had a nanoshell-assisted tumor photothermal treatment, and dog 5, a control case that had an identical photothermal treatment without nanoshells. Figure 2 shows the results of laser treatment of dog 4. Figure 2*A* is an axial MR-DCE image at the plane of the inoculated tumor taken ~1 hour before nanoshell infusion using Magnevist to highlight rates of blood wash-in and wash-out, indicative of neoplasia. The tumor, indicated by the arrows, was bilobed and situated in the right parietal lobe. The two dark rectangular regions abutting the superior portion of the skull indicate the position of the two Bone Anchors used to inoculate the tumor (right) and the sham inoculation (left) and to introduce and secure the laser catheter in the brain. Figure 2*B* is a MR-DCE image of the same plane taken 48 hours after laser treatment, immediately before sacrifice. The single laser treatment of the inferior of the two tumor lobes is easily distinguished from the untreated superior lobe as indicated by the arrow. The superior lobe takes up the Magnevist contrast agent, indicating intact blood perfusion. The inferior lobe shows only a ring of contrast, indicating the presence of edema around the periphery of the ablated tumor lobe. The track of the laser catheter and the laser treatment of the normal brain in the left hemisphere produced insufficient damage to be seen in these images. The superior lobe of the tumor was left untreated to provide means of comparison in the MR-DCE imaging and to permit harvest of intact nanoshell-containing tumor for EA analysis.

Figure 2*C* and *D* shows gross pathology transverse slices of the left and right hemispheres, respectively, of the brain shown in Fig. 2*A* and *B*. Arrows indicate the location of the passage of the laser catheter into the plane of the image. The left hemisphere in Fig. 2*C* shows a small damage zone, indicating the passage of the optical fiber catheter, but no thermal damage sequelae. The right hemisphere in Fig. 2*D* shows that thermal damage has been confined to the tumor and an area immediately adjacent to it. Significantly, the path of the laser catheter was caudal and lateral to the ablated tumor at this plane as indicated by the arrow, showing that the isotropically irradiating laser fiber was external to the tumor. Caudal to the fiber, the normal brain tissue has remained intact. Damage rostral (right in the image) to the fiber, by contrast, indicates complete thermal ablation of the inferior lobe of the tumor. The original cTVT is shown circumscribed by the inner ring, the zone of thermal ablation and complete cell death by the middle ring, and a region of edema by the outer ring. From histopathology of all of the treated dogs, we noted cellular necrosis extended from 0.5 to 4 mm outward from the identifiable tumor boundary, indicating thermal diffusion from the particle-ablated areas.

Figure 3 shows the clinical results of an identical laser treatment on control dog (dog 5 in Table 1) that was given a blood-volume comparable infusion of the 10% trehalose vehicle without nanoshells. Figure 3*A* is an axial view of a MR-DCE image at the plane of the inoculated tumor taken ~1 hour before the nanoshell infusion.

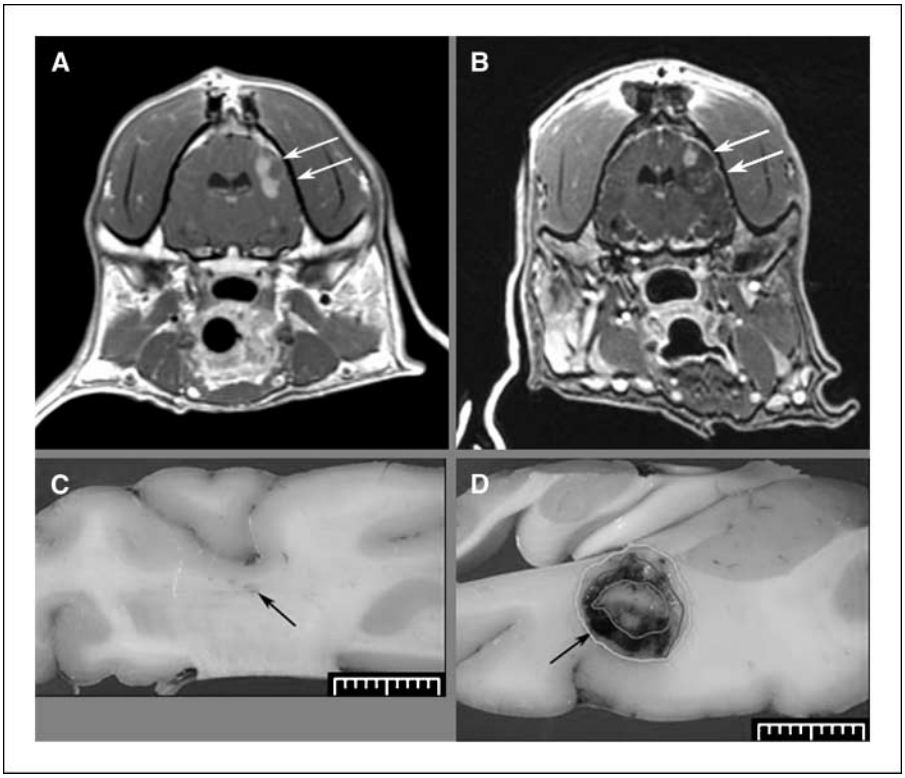

Figure 2. AuroLase treatment of cTVT in brain of dog 4. *A, arrows,* MR-DCE axial image of dog brain showing contrast enhancement of bilobed tumor along inoculation track. *B, arrows,* MR-DCE axial image of dog brain after laser treatment showing ablation of inferior lobe. *C,* control cerebral hemisphere showing no ablation in normal brain. *Arrow,* fiber insertion point. *D,* ablation zones (inner ring = boundary of tumor, middle ring = boundary of thermal necrosis, outer ring = boundary of zone of edema) around nanoshell-containing tumor. *Arrow,* fiber insertion point.

The tumor has two connected lobes (indicated by arrows) along the inoculation track. Figure 3*B* is a MR-DCE image of the same plane taken 48 hours after laser treatment. The single laser treatment has resulted in a small ablation zone lateral to the fiber track indicated by the arrow as a small dark region. Fig. 3*C* and *D* shows gross pathology coronal slices of the left and right hemispheres, respectively, of the brain shown in Fig. 3*A* and *B*. Arrows indicate the location of the passage of the laser catheter into the plane of

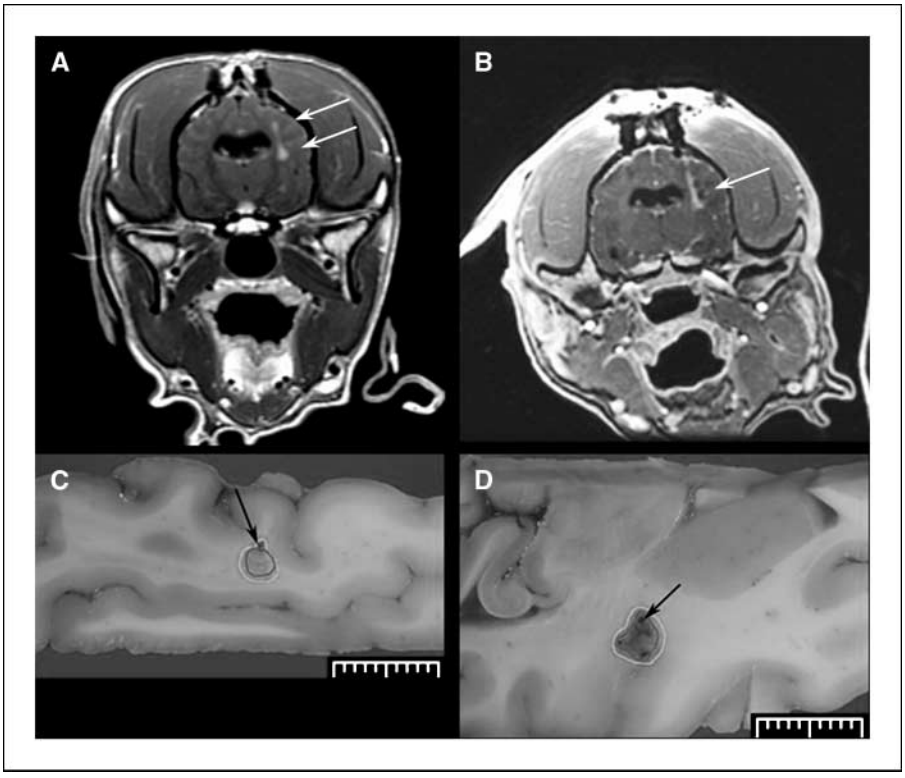

Figure 3. Laser treatment of cTVT in the brain of dog 5. *A, arrows,* MR-DCE axial image of dog brain showing contrast enhancement of elongated tumor along inoculation track. *B, arrow,* MR-DCE axial image of dog brain after laser treatment showing small ablation zone. *C,* small ablation zone in normal white matter. *Arrow,* fiber insertion point. *D,* ablation zone around control tumor (inner ring = boundary of area of thermal necrosis, outer ring = boundary of edema). *Arrow,* fiber insertion point.

the image, medial to the ablation zone in both cases. Zones of thermal ablation and complete cell death are circumscribed by the inner ring and surrounding regions of edema by the outer ring. The damage zones in this case are roughly comparable with thermal damage being done to both normal brain and cTVT.

Discussion

We have presented here a pilot study showing a proof of concept that nanoshells combined with laser-based thermotherapy can be effective for highly specific brain tumor ablation. The primary goal of this study was to evaluate the feasibility of the treatment. Consequently, therapeutic efficacy that would require a priori knowledge of nanoshell accumulation in the target tumor as well as laser dose optimization for treatment of the entire tumor and interactive adjustment of the laser exposure as opposed to a fixed exposure (for reproducibility) was not addressed and awaits more detailed research. We have shown that passively delivered, 150-nm nanoshells specifically accumulate in the cTVT allograft brain tumor model and that laser activation of the nanoshells results in selective photothermal ablation of tumor tissue using laser fluences that are tissue sparing in the absence of nanoshells.

The surgery, nanoshell infusion, MRI, and laser treatment portions of this study proceeded relatively smoothly. The largest difficulty proved to be the reliability of the inoculation and growth of the cTVT tumors in dog. Of the nine inoculations, five succeeded in brain, five succeeded s.c., but only three succeeded in both locations. The cTVT used in this study was harvested from and consistently passed successfully through SCID mice, so it is likely that the problem with inoculation had more to do with inadequate immunosuppression of the dogs than with tumor viability.

The nanoshell particles used in this study were designed to absorb optical radiation in the vicinity of 800 nm. The selective accumulation of these particles in the neovasculature of the growing cTVT had the effect of increasing the local optical extinction leading to increased deposition of photon energy in neovascularized tissue leading to tissue-specific ablation. The high gold concentration in viable cTVT additionally shows that cTVT microvasculature possesses pores or fenestrations into which the 150-nm nanoshells may be inserted (25). Primary glioblastomas also possess microvasculature pores, which may, depending on their size and the specific tumor type, be exploited by PEGylated nanoparticles (26). There is no evidence that 150-nm nanoshells are endocytosed by tumor cells; transmission electron microscopy analysis indicates their accumulation along capillary walls.

The graph in Fig. 4 compares EA measurements of tissue gold content for cTVT tissue and normal canine white matter. Gold concentrations in untreated, viable cTVT taken from brain was measured at 22.5 $\pm$ 24.0 μg/g of tissue weight, 2.2 times the 10.3 $\pm$ 5.6 μg/g concentration in cTVT inoculated s.c. on the flank. Also of interest is the gold concentration of 11.6 $\pm$ 10.9 μg/g remaining in ablated portions of tumor 48 hours after laser treatment. Two samples of white matter taken from dogs inoculated with nanoshells showed a gold concentration of 0.144 $\pm$ 0.143 μg/g, indicating a baseline nanoshell concentration 156-fold below that in tumor.

The 15-nm-thick gold shell over the 120-nm-diameter silica core implies a gold mass of 1.66e−14 g/nanoshell. The EA data in Fig. 4 thus suggest nanoshell concentrations of 1.36e9/g tissue weight for cTVT in brain, 6.18e8/g in cTVT in flank, 6.96e8/g in ablated cTVT, and 8.65e6/g in normal brain. This has important implications for the laser dosimetry in that nanoshells provide enhanced optical absorption at the therapeutic laser wavelength. Although the 800-nm absorption peak for nanoshells falls within the therapeutic window where endogenous optical attenuation is at a minimum, hemoglobin is still a substantial absorber with an absorption coefficient $\mu_a \sim 0.5\ cm^{-1}$ (assuming a 6.5% tissue blood volume). Nanoshells, which both scatter and absorb light, add to the optical extinction in tumor tissue where they accumulate. The nanoshell concentrations above add 0.51 $\pm$ 0.54 absorbance to the cTVT extinction in brain and 0.0033 $\pm$ 0.0033 absorbance to normal

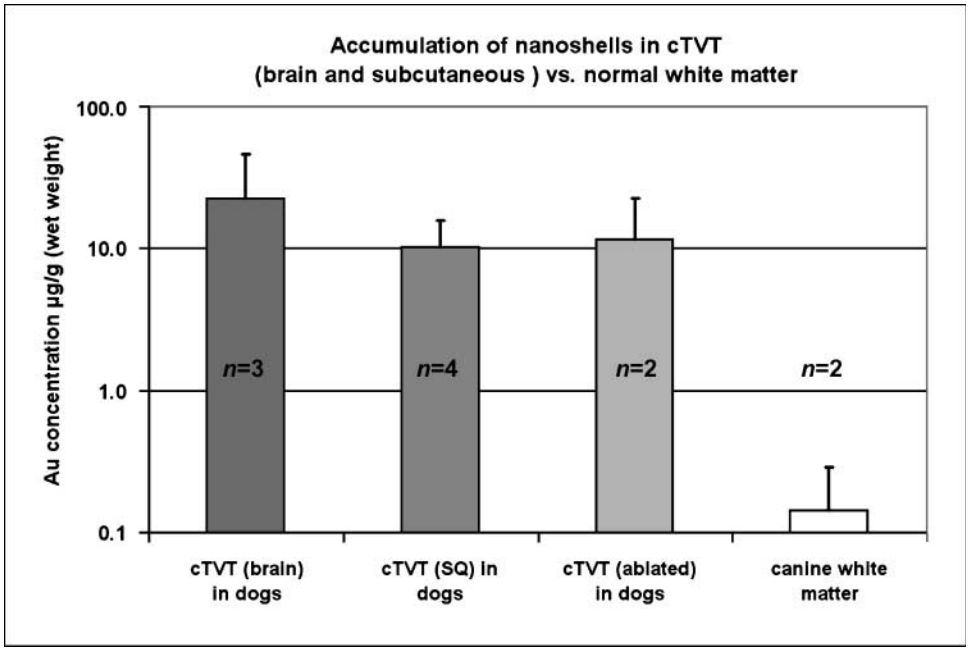

Figure 4. EA of gold content in cTVT and normal canine white matter.

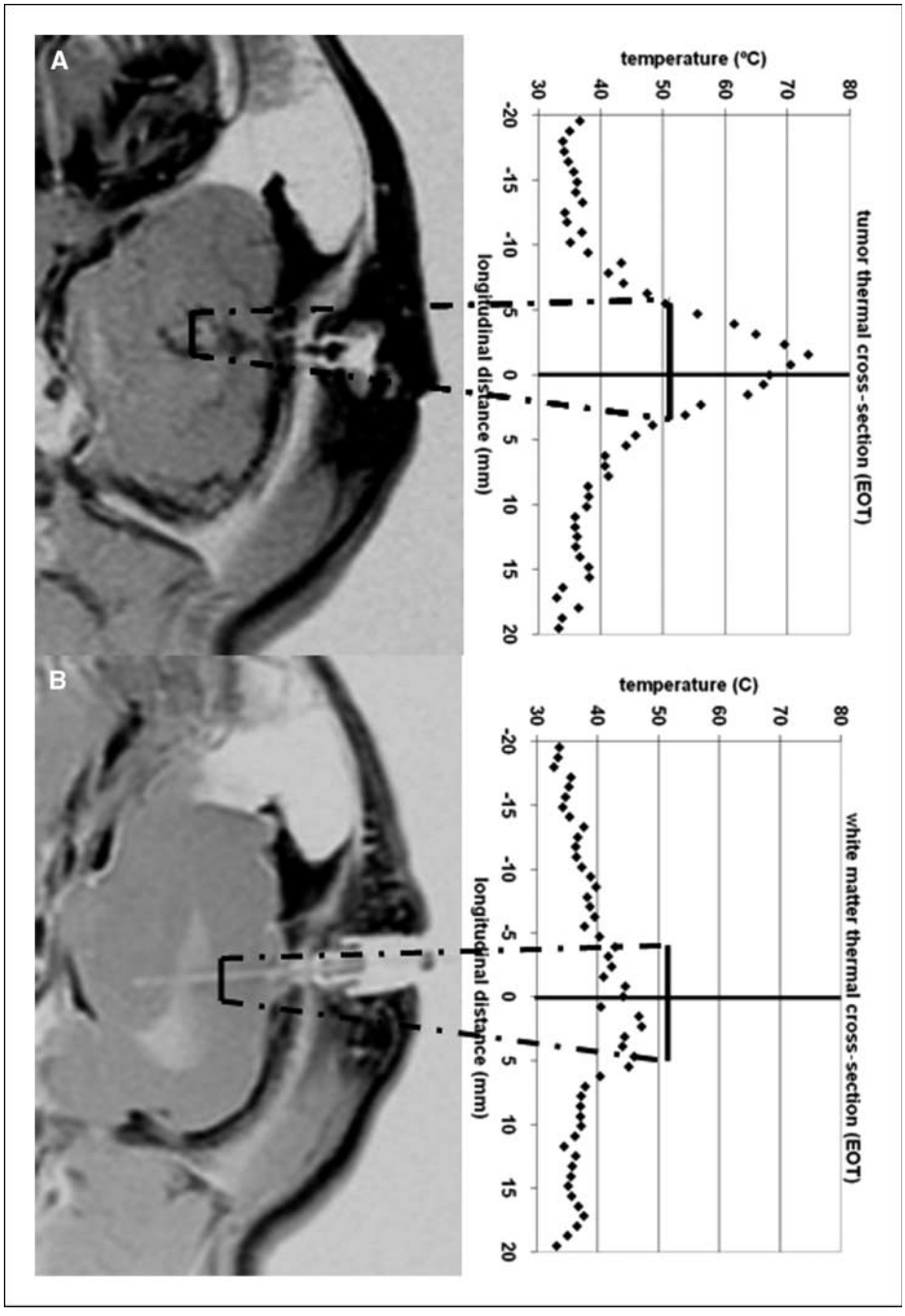

Figure 5. Comparison of thermal ablation of nanoshell-containing tumor with hyperthermia of normal white matter. *A,* MR-DCE sagittal image of dog 4 brain right hemisphere showing the ablated inferior tumor lobe surrounded by edema (*black ring*) at left and the end-of-treatment (*EOT*) temperature cross-section of the tumor at right. *B,* MR-DCE sagittal image of dog 4 left hemisphere showing native white matter at left and the EOT temperature cross-section of the white matter at right.

white matter. Although this analysis would clearly benefit from a larger sample size, it is nevertheless clear that the enhanced optical extinction resulting from the accumulation of nanoshells within the cTVT reduces the photon mean free path by ~0.85 cm, substantially confining the source of the resultant heat to tissue containing nanoshells.

In this study, we have endeavored to handle the dogs and tumors consistently and to maintain a rigorous pretreatment regimen. Nevertheless, nanoshell accumulation in intracranial cTVT varied widely, albeit 156-fold greater than in normal white matter. In spite of the variation in nanoshell accumulation indicated in Table 1, the plateau temperatures for intracranial tumors for which nanoshells had been infused [65.8 ± 4.1°C (n = 4)] were greater than the tumor for which only the test vehicle had been infused (53.1°C) and statistically distinct from the plateau temperatures for white matter in all cases. The difference in plateau temperatures between the nanoshell tumors and the contralateral white matter was 14.9 ± 6.8°C (n = 4). The statistics for the peak temperatures in normal white matter bears examination. As may be noted in Table 1, the plateau temperatures for white matter excluding dog 2 are a subablative 48.6 ± 1.1°C (n = 5; refs. 27, 28). Including dog 2, the white matter plateau temperatures rise to the ablative 50.0 ± 3.6°C (n = 6). The 57.1°C white matter temperature plateau for dog 2 resulted from the hemorrhage of a blood vessel at the base of a deep sulcus through which the optical fiber had passed, thus showing the ablative potential of pooled blood in the vicinity of the

laser source even under irradiation conditions that were nominally subablative.

The case of dog 4 highlights two principal features of using nanoparticle-assisted laser tumor ablation: (*a*) that enhanced optical absorption by nanoparticles leads to tumor-specific generation of ablative levels of heat and (*b*) that the 3.5-W, 3-minute NIR laser dosimetry is nonablative in normal white matter and leads to a steep temperature gradient at the tumor boundary, which tends to confine thermal damage to nanoshell-containing tissue. Figure 5 shows a comparison between the results of identical laser treatments in the tumor-containing right hemisphere (Fig. 5*A*) and normal white matter in the left hemisphere (Fig. 5*B*). On the left are sagittal (rostral toward the top, caudal toward the bottom) MR *T1* images of the brain and surrounding tissue. On the right are temperature measurements derived from the real-time phase images at the end of the 3-minute laser irradiation. Each line of thermal data was chosen to transect the plane of maximum temperature for the thermal lesion in each case. The MR images are shown in reverse color for clarity. Figure 5*A* shows an MR image slice through the center of the ablated tumor where from Table 1 we note nanoshells had accumulated producing a gold concentration of 15.5 μg/g of tumor corresponding to ~9.34e9 nanoshells/gram of tumor. The graph at right illustrates that the damage margin extends to the edge of the dark ring (edema as detected by MR-DCE), 7 pixels (5.5 mm) rostral and 4 pixels (3.1 mm) caudal to the position of the optical fiber. This led to a damage zone 8.6 mm along the sagittal plane as seen in the gross pathology image in Fig. 2*D*, and resulted in tissue necrosis of the treated inferior lobe of the tumor surrounded by a 1- to 2-mm-wide edematous ring. Figure 5*B* shows a MR image slice through the plane of the optical fiber, visible as the light-colored line passing through the skull bolt at right and proceeding through the parietal lobe (leftward in the image). The graph at right indicates the subablative hyperthermia of normal white matter, which, as shown in the gross pathology image in Fig. 2*C*, resulted in no tissue necrosis. As indicated by Table 1, 3.5 W of NIR laser power will result in localized heating of white matter resulting in mild hyperthermia over the course of a 3-minute treatment (29). Additional tests (data not shown) at 3.8 W produced regions of heating in white matter with core temperatures ranging from 54°C to 62°C resulting in ablative lesions. It would seem, therefore, that 3.5 W of 808-nm radiation emitted from a 1-cm-long diffusing optical fiber is just below the threshold for ablative damage in unmodified brain tissue.

The enhanced vascularity of the cTVT tumor that enabled its visualization with MR-DCE also suggests an increased optical absorption due to enhanced blood volume. Simultaneously, the enhanced blood volume suggests the possibility of enhanced perfusion cooling of the tumor tissue. The thermal ablation produced in the control brain shown in Fig. 3 suggests that the increased absorption is the dominant effect—that any increase in perfusion cooling was insufficient to offset the absorption by blood of NIR photon energy from the laser.

Additional studies will be necessary to elucidate the efficacy of nanoshell-assisted photothermal ablation in different classes of tumors to add statistical power to the results presented here. In this pilot study, we have developed a procedure by which systemically infused nanoshells, in conjunction with a minimally invasive percutaneous optical fiber delivering low-dose NIR radiation, enabled us to selectively ablate orthotopically situated tumors in the brain with a minimal margin of damage to adjacent normal brain tissue. Systemic delivery of nanoshells permitted nanoshell accumulation in cTVT without restriction on tumor location, and the lack of a biochemical or metabolic interaction with tissue should make it possible for nanoshell-assisted treatment to be used in conjunction with other therapies.

Disclosure of Potential Conflicts of Interest

Nanospectra Biosciences manufactures AuroLase Particles and has an Investigational Device Exemption from the Food and Drug Administration to develop AuroLase Therapy for recurrent tumors of the head and neck.

Acknowledgments

Received 7/2/2008; revised 10/28/2008; accepted 11/17/2008.

Grant support: This work was funded by National Science Foundation grant OII-0548741 and is based on work previously funded by National Institute of Standards and Technology Advanced Technology Program award 70NANB4H3040.

The costs of publication of this article were defrayed in part by the payment of page charges. This article must therefore be hereby marked *advertisement* in accordance with 18 U.S.C. Section 1734 solely to indicate this fact.

We thank Dr. Donna J. O'Kelly (The University of Texas) for providing EA of gold content for this work and Krystina Sang for maintaining the cTVT tumor line.

References

1. Maldaun MV, Aguiar PH, Lang F, Suki D, Wildrick D, Sawaya R. Radiosurgery in the treatment of brain metastases: critical review regarding complications. Neurosurg Rev 2008;31:1–8; discussion -9.
2. Fisher JL, Schwartzbaum JA, Wrensch M, Wiemels JL. Epidemiology of brain tumors. Neurol Clin 2007;25:867–90, vii.
3. Eichler AF, Loeffler JS. Multidisciplinary management of brain metastases. Oncologist 2007;12:884–98.
4. Maeda H. The enhanced permeability and retention (EPR) effect in tumor vasculature: the key role of tumor-selective macromolecular drug targeting. Adv Enzyme Regul 2001;41:189–207.
5. Ishida O, Maruyama K, Sasaki K, Iwatsuru M. Size-dependent extravasation and interstitial localization of polyethyleneglycol liposomes in solid tumor-bearing mice. Int J Pharm 1999;190:49–56.
6. Kong G, Braun RD, Dewhirst MW. Hyperthermia enables tumor-specific nanoparticle delivery: effect of particle size. Cancer Res 2000;60:4440–5.
7. Oldenburg SJ, Jackson JB, Westcott SL, Halas NJ. Infrared extinction properties of gold nanoshells. Appl Phys Lett 1999;75:2897–9.
8. Jackson JB, Halas NJ. Surface-enhanced Raman scattering on tunable plasmonic nanoparticle substrates. Proc Natl Acad Sci U S A 2004;101:17930–5.
9. James WD, Hirsch LR, West JL, O'Neal DP, Payne JD. Application of INAA to the build-up and clearance of gold nanoshells in clinical studies in mice. J Radioanal Nucl Chem 2007;271:455–9.
10. Hirsch LR, Stafford RJ, Bankson JA, et al. Nanoshell-mediated near-infrared thermal therapy of tumors under magnetic resonance guidance. Proc Natl Acad Sci U S A 2003;100:13549–54.
11. O'Neal DP, Hirsch LR, Halas NJ, Payne JD, West JL. Photo-thermal tumor ablation in mice using near infrared-absorbing nanoparticles. Cancer Lett 2004;209:171–6.
12. Stern JM, Stanfield J, Kabbani W, Hsieh JT, Cadeddu JA. Selective prostate cancer thermal ablation with laser activated gold nanoshells. J Urol 2008;179:748–53.
13. Diagaradjane P, Shetty A, Wang J, et al. Modulation of *in vivo* tumor radiation response via gold nanoshell-mediated vascular-focused hyperthermia: characterizing an integrated antihypoxic and localized vascular disrupting targeting strategy. Nano Lett 2008;8:1492–500.
14. Oldenburg SJ, Averitt RD, Westcott SL, Halas NJ. Nanoengineering of optical resonances. Chem Phys Lett 1998;288:243–7.
15. Duff DG, Baiker A. A new hydrosol of gold clusters. 1. Formation and particle size variation. Langmuir 1993;9:2301–9.
16. Lindstedt L, Schaeffer PJ. Use of allometry in predicting anatomical and physiological parameters of mammals. Lab Anim 2002;36:1–19.
17. Kangasniemi M, McNichols RJ, Bankson JA, Gowda A, Price RE, Hazle JD. Thermal therapy of canine cerebral tumors using a 980 nm diode laser with MR temperature-sensitive imaging feedback. Lasers Surg Med 2004;35:41–50.
18. Rivera B, Ahrar K, Kangasniemi MM, Hazle JD, Price RE. Canine transmissible venereal tumor: a

large-animal transplantable tumor model. Comp Med 2005;55:335–43.
19. Alfano RR, Demos SG, Gayen SK. Advances in optical imaging of biomedical media. Ann N Y Acad Sci 1998; 838:248–71.
20. Weissleder R. A clearer vision for *in vivo* imaging. Nat Biotechnol 2001;19:316–7.
21. Stafford RJ, Price RE, Diederich CJ, Kangasniemi M, Olsson LE, Hazle JD. Interleaved echo-planar imaging for fast multiplanar magnetic resonance temperature imaging of ultrasound thermal ablation therapy. J Magn Reson Imaging 2004;20:706–14.
22. McNichols RJ, Gowda A, Kangasniemi M, Bankson JA, Price RE, Hazle JD. MR thermometry-based feedback control of laser interstitial thermal therapy at 980 nm. Lasers Surg Med 2004;34:48–55.
23. Thomas DL, Lythgoe MF, Pell GS, Calamante F, Ordidge RJ. The measurement of diffusion and perfusion in biological systems using magnetic resonance imaging. Phys Med Biol 2000;45:R97–138.
24. Jones TC, Hunt RD, King NW. Introduction: Cells: death of cells and tissues. In: Veterinary pathology. 6th ed. Hoboken: Blackwell Publishing; 1997.
25. Provenzale JM, Mukundan S, Dewhirst M. The role of blood-brain barrier permeability in brain tumor imaging and therapeutics. AJR Am J Roentgenol 2005;185:763–7.
26. Hobbs SK, Monsky WL, Yuan F, et al. Regulation of transport pathways in tumor vessels: role of tumor type and microenvironment. Proc Natl Acad Sci U S A 1998; 95:4607–12.
27. McNichols RJ, Kangasniemi M, Gowda A, Bankson JA, Price RE, Hazle JD. Technical developments for cerebral thermal treatment: water-cooled diffusing laser fibre tips and temperature-sensitive MRI using intersecting image planes. Int J Hyperthermia 2004;20:45–56.
28. Sapareto SA, Dewey WC. Thermal dose determination in cancer therapy. Int J Radiat Oncol Biol Phys 1984; 10:787–800.
29. Dewhirst MW, Viglianti BL, Lora-Michiels M, Hanson M, Hoopes PJ. Basic principles of thermal dosimetry and thermal thresholds for tissue damage from hyperthermia. Int J Hyperthermia 2003;19:267–94.